MATERIAL SCIENCE / МАТЕРИАЛОВЕДЕНИЕ

UDC 669.1
DOI 10.17073/0368-0797-2023-4-434-441

Original article
Оригинальная статья

Effect of morphology and volume fraction of δ-ferrite on hydrogen embrittlement of stainless steel produced by electron beam additive manufacturing

M. Yu. Panchenko, K. A. Reunova, A. S. Nifontov,
E. A. Kolubaev, E. G. Astafurova ✉

Institute of Strength Physics and Materials Science, Siberian Branch of Russian Academy of Sciences (2/4 Akademicheskii Ave., Tomsk 634055, Russian Federation)

✉ elena.g.astafurova@ispms.ru

Abstract. The authors studied the influence of volume fraction and morphology of δ-ferrite on hydrogen embrittlement of austenitic stainless steel 08Kh19N9T obtained by electron beam additive manufacturing. It is experimentally shown that in additively-manufactured samples, long lamellae of δ-ferrite form a dense "net" of interphase boundaries (austenite/δ-ferrite, the volume fraction of the δ-phase is 20 %) and contribute to the hydrogen accumulation. Also, being the "easy" ways for the diffusion of hydrogen atoms, the dendritic lamellae of ferrite provide hydrogen transport deep into the samples. Post-production solid-solution treatment (at T = 1100 °C, 1 h) leads to a significant decrease in the fraction of δ-ferrite in steel (up to 5 %) and partial dissolution of dendritic lamellae. A decrease in the volume fraction of ferrite and a change in its morphology hinder the diffusion of hydrogen deep into the samples and its accumulation during electrolytic hydrogen-charging and subsequent deformation. It contributes to a decrease in the total concentration of hydrogen dissolved in the steel samples. Despite the lower concentration of dissolved hydrogen in the solid-solution treated samples, the solid-solution strengthening by hydrogen atoms is higher ($\Delta\sigma^{H}_{0.2}$ = 73 MPa) than for the initial samples with a high content of δ-ferrite ($\Delta\sigma^{H}_{0.2}$ = 55 MPa). The solid-solution treated samples are characterized by a smaller thickness of the brittle surface hydrogen-charged layer and a lower hydrogen embrittlement index compared to the post-produced samples (D_H = 55 ± 12 μm, I_H = 32 % for initial samples and D_H = 29 ± 7 μm, I_H = 24 % for samples after post-production solid-solution treatment).

Keywords: austenitic steel, additive technologies, hydrogen embrittlement, δ-ferrite, fracture, microstructure, mechanical properties

Acknowledgements: The work was performed within the framework of the state task of the Institute of Strength Physics and Materials Science, Siberian Branch of Russian Academy of Sciences, project No. FWRW-2022-0005. The study was conducted using the equipment of the Institute of Strength Physics and Materials Science, Siberian Branch of Russian Academy of Sciences ("Nanotech" center).
The authors express their gratitude to S.V. Astafurov, G.G. Maier, E.V. Mel'nikov, V.E. Rubtsov and S.Yu. Nikonov for their help in conducting experimental works and assistance in obtaining materials.

For citation: Panchenko M.Yu., Reunova K.A., Nifontov A.S., Kolubaev E.A. Astafurova E.G. Effect of morphology and volume fraction of δ-ferrite on hydrogen embrittlement of stainless steel produced by electron beam additive manufacturing. *Izvestiya. Ferrous Metallurgy*. 2023;66(4):434–441. https://doi.org/10.17073/0368-0797-2023-4-434-441

Влияние морфологии и объемной доли δ-феррита на водородное охрупчивание нержавеющей стали 08Х19Н9Т, полученной методом электронно-лучевого аддитивного производства

М. Ю. Панченко, К. А. Реунова, А. С. Нифонтов,
Е. А. Колубаев, Е. Г. Астафурова ✉

Институт физики прочности и материаловедения Сибирского отделения РАН (Россия, 634055, Томск, пр. Академический, 2/4)

elena.g.astafurova@ispms.ru

Аннотация. В настоящей работе изучено влияние объемной доли и морфологии δ-феррита на закономерности водородного охрупчивания образцов аустенитной нержавеющей стали 08Х19Н9Т, полученной методом электронно-лучевого аддитивного производства. Экспериментально показано, что в аддитивно-изготовленных образцах длинные дендритные ламели δ-феррита формируют плотную «сетку» межфазных границ (аустенит – δ-феррит, объемная доля δ-фазы составляет 20 %) и способствуют накоплению водорода. Дендритные ветви феррита являются «легкими» путями для диффузии атомов водорода и поэтому обеспечивают его транспорт в глубь образцов. Постпроизводственная термическая обработка (при температуре 1100 °С, в течение 1 ч) приводит к значительному уменьшению доли δ-феррита в аддитивно-полученной стали (до 5 %) и частичному растворению дендритных ламелей. Уменьшение объемной доли феррита и изменение его морфологии затрудняет диффузию водорода в глубь образца и его накопление в процессе электролитического насыщения и последующей деформации, способствует понижению общей концентрации растворенного в образцах водорода. Несмотря на меньшую концентрацию растворенного водорода в образцах, подвергнутых термообработке, твердорастворное упрочнение атомами водорода оказывается больше ($\Delta\sigma^{H}_{0,2}$ = 73 МПа), чем для исходных образцов с высокой долей δ-феррита ($\Delta\sigma^{H}_{0,2}$ = 55 МПа). Также образцы после постпроизводственной термической обработки характеризуются меньшей толщиной хрупкого поверхностного наводороженного слоя D_H и более низким коэффициентом водородного охрупчивания I_H по сравнению с исходными аддитивно-полученными образцами (D_H = 55 ± 12 мкм, I_H = 32 % для исходных образцов и D_H = 29 ± 7 мкм, I_H = 24 % для образцов после постпроизводственной термической обработки).

Ключевые слова: аустенитная сталь, аддитивные технологии, водородное охрупчивание, δ-феррит, разрушение, микроструктура, механические свойства

Благодарности: Работа выполнена в рамках государственного задания Института физики прочности и материаловедения Сибирского отделения РАН, тема № FWRW-2022-0005.
Исследования проведены с использованием оборудования ЦКП «Нанотех» (Институт физики прочности и материаловедения Сибирского отделения РАН). Авторы выражают благодарность к.ф.-м.н. С.В. Астафурову, к.ф.-м.н. Г.Г. Майер, Е.В. Мельникову, к.ф.-м.н. В.Е. Рубцову и к.ф.-м.н. С.Ю. Никонову за помощь в проведении экспериментальных исследований и получении материалов.

Для цитирования: Панченко М.Ю., Реунова К.А., Нифонтов А.С., Колубаев Е.А., Астафурова Е.Г. Влияние морфологии и объемной доли δ-феррита на водородное охрупчивание нержавеющей стали 08Х19Н9Т, полученной методом электронно-лучевого аддитивного производства. *Известия вузов. Черная металлургия*. 2023;66(4):435–441. https://doi.org/10.17073/0368-0797-2023-4-434-441

Introduction

Additive manufacturing (AM) represents a rapidly advancing domain encompassing both science and industry. It introduces a transformative approach to crafting intricate components and parts for mechanisms characterized by intricate configurations, a feat previously unattainable using conventional manufacturing techniques. The application of additive technologies holds significant potential within the burgeoning sphere of hydrogen energy. This encompasses endeavors related to hydrogen storage, transportation, and the fabrication of essential components like hydrogen fuel cells and vehicles. Stable austenitic stainless steels exhibit the highest resistance to hydrogen's adverse effects when compared to other steel categories [1; 2]. Their favorable weldability and moderate cost make them an appealing choice for utilization as foundational materials within additive technologies [3; 4]. Nevertheless, when devising components intended for operation in aggressive hydrogen-rich environments, it becomes imperative to consider the unique microstructural attributes intrinsic to this steel category that manifest during the AM process. These attributes take into account the anisotropic nature of grain structure [5; 6] and formation of the secondary phases [7 – 9].

Currently, the subject of hydrogen embrittlement in steel samples produced through AM techniques remains inadequately explored in published literature, with occasional inconsistencies in the available data. The study [10] revealed that austenitic steel AISI 304L, fabricated using laser powder AM technology, is more resistant to hydrogen embrittlement compared to conventionally obtained rolled steel. This enhanced resistance is attributed to the development of a stable austenitic phase that is resistant to phase transitions, as well as the distinctive texture of the steel brought about during powder sintering. Research presented in [11] demonstrated the heightened vulnerability of martensitic aging steel produced through selective laser melting to hydrogen embrittlement. Stainless steel 17-4 PH, featuring a coarse crystalline ferritic structure and manufactured via laser additive technologies, is more prone to the adverse effects of hydrogen than its cast counterpart [12]. Conversely, for ferritic steel 09G2S, additively produced steel using the electron beam AM method exhibits a weaker susceptibility to hydrogen embrittlement than its cast equivalent [13].

In comprehending the reasons behind the degradation of mechanical properties induced by hydrogen in additively manufactured austenitic steels – known for their resistance to hydrogen embrittlement – grasping the role of key microstructural aspects in these processes becomes crucial. Particularly, samples of austenitic steels generated through electron beam AM methods exhibit distinctive characteristics: an anisotropic grain structure and a notable proportion of the δ-phase (approximately 20 %) [6 – 8]. This study aims to strategically manipulate the morphology and volume fraction of δ-ferrite within 08Kh19N9T steel samples produced via electron beam additive manufacturing (EBAM), while keeping other structural parameters (primarily the size of austenite grains) unchanged [6].

The objective of this research is to establish patterns concerning the hydrogen embrittlement of austenitic steel

08Kh19N9T manufactured using the EBAM technique, contingent on the morphology and content of δ-ferrite in its structure.

Experimental methods

For the EBAM process, we utilized an industrial wire composed of austenitic stainless steel (ASS) 08Kh19N9T, with the following chemical composition (wt. %): Cr 17.7; Ni 9.7; Mn 1.1; Ti 0.8; Si 0.6; C 0.08; with iron constituting the remainder (wire diameter 1.2 mm). The electron beam additive manufacturing was executed within a vacuum chamber, employing the subsequent parameters: accelerating voltage of 30 kV, wire feed speed set at 180 mm/min, beam sweep spanning 45×45 mm, scanning frequency of 1 kHz, and electron beam current of 45 mA. The accumulation of material layers transpired atop an austenitic steel substrate, resulting in a final geometric configuration of the steel billet measuring 110×6×30 mm.

For the purpose of uniaxial static tension tests, flat samples resembling double blades were fashioned, with the working part dimensions at 12×3×1.5 mm. These samples were extracted from an additively manufactured steel wall. A portion of the samples were assessed in their initial state – directly following additive growth (AM-ASS) – while another subset underwent annealing at 1100°C for 1 hour, succeeded by water quenching (AM-ASS + HT). Surface treatment encompassed mechanical grinding and electrolytic polishing using a solution of 25 g CrO_3 and 200 ml H_3PO_4.

Microstructural analysis of the obtained samples was conducted using optical (OM) and transmission electron microscopy (TEM), utilizing Altami MET 1C and Jeol JEM 2100 microscopes, respectively. The magnetic phase analysis (MPA) technique was employed, specifically with an MVP-3 ferritometer (Kropus, Russia) to determine the volume fraction of the δ phase (V_δ).

Electrolytic hydrogenation was executed in a 3 % NaCl aqueous solution containing 3 g/L NH_4SCN. This procedure spanned 50 h at a current density of 50 mA/cm^2. Thermal desorption spectroscopy (TDS) investigations – centered on evaluating the rate of hydrogen liberation from specimens during gradual heating – were conducted using an automated Gas Reaction Controller LBP system (Advanced Materials Research, USA). This was executed with a heating rate of 360 °C/h, within a temperature span ranging from 25 to 400 °C. Tensile tests were carried out at room temperature, maintaining an initial strain rate of $5\cdot10^{-4}$ s^{-1}. The testing was performed employing an LFM-125 universal electromechanical testing machine (Walter+Bai AG, Switzerland). Subsequently, the fracture surfaces of the samples were meticulously analyzed using a LEO EVO 50 scanning electron microscope (SEM) (Zeiss, Germany). To estimate the thickness of the brittle hydrogen-induced layer, SEM images acquired from the fracture surfaces of hydrogenated samples were employed. The secant method was utilized for this purpose, wherein the secants were oriented perpendicular to the hydrogenated layer.

Results and discussion

Fig. 1 presents optical microscopy (OM) and transmission electron microscopy (TEM) images of samples produced via the EBAM process. Both categories of samples exhibit a dual-phase (γ + δ) configuration. Notably, the δ-ferrite lamellae emergence of the δ phase within the structure of additively manufactured samples is attributed to distinct characteristics of the EBAM process, encompassing the intricate, multistage thermal history of layers and the overall billet, as well as the diminution of nickel content within the melt, among other factors [7; 9; 14]. Subsequent heat treatment (1100 °C, 1 h) induces a reduction in the δ-ferrite con-

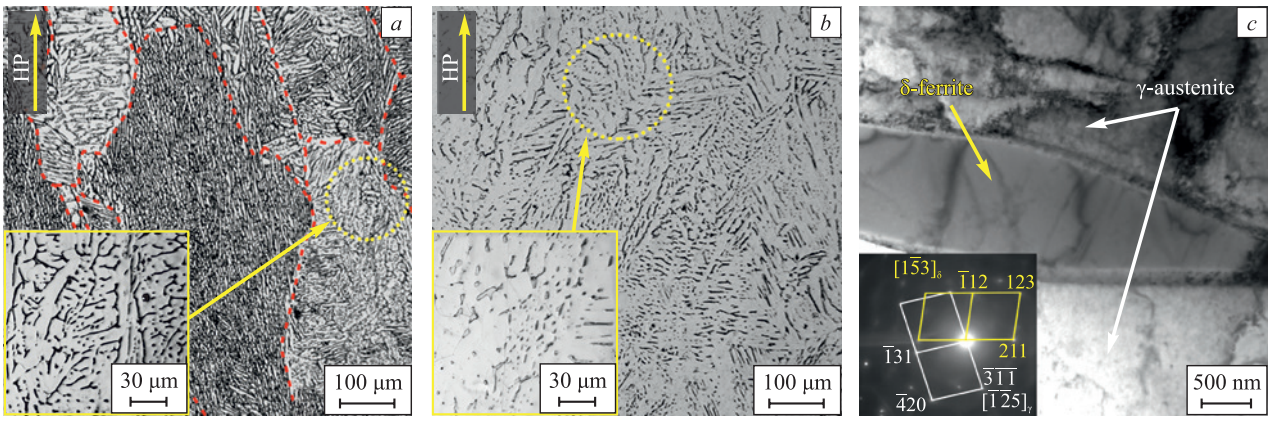

Fig. 1. OM images (*a*, *b*) and SEM image (*c*) of the samples of additive manufactured austenic stainless steel (AM-ASS) (*a*) and AM-ASS + heat treatment (HT) (*b*, *c*):
HP – direction of growth of the electron beam addive manufactured (EBAM) billet; --- – boundaries of austenitic grains

Рис. 1. ОМ-изображения (*a*, *b*) и ПЭМ-изображение (*c*) образцов АП-АНС (*a*) и АП-АНС + ТО (*b*, *c*):
НР – направление роста ЭЛАП-заготовки; --- – границы аустенитных зерен

tent while simultaneously altering its morphology – a phenomenon exhaustively elucidated in [6]. In specific, the heat treatment results in the formation of a dendritic structure of δ-ferrite, characterized by an average lamella thickness of 0.8 ± 0.4 μm within the AM-ASS samples. Following heat treatment, prolonged continuous branches (lamellae) of δ-ferrite experience partial dissolution, giving rise to non-equiaxed δ-phase grains (particles). These new grains exhibit an average thickness and length of 1.3 ± 0.5 and 6.2 ± 3.1 μm, respectively (Fig. 1, *b*). Consequently, the volume fraction of ferrite diminishes from 20 % to 5 % after the heat treatment, while the grain structure of the principal phase (austenite) remains unaffected [6]. Thus, the heat treatment exclusively influences the morphology and volume fraction of the ferrite phase, maintaining all other structural parameters unaltered.

For hydrogenated AM-ASS and AM-ASS + HT samples, their thermal desorption (TDS) spectra depict a sole peak at T_{max} = 160 – 165 °C (Fig. 2, *a*). This low-temperature peak corresponds to the release of hydrogen atoms from the crystal lattice and various weak, reversible traps possessing low activation energies. These encompass grain boundaries, interfacial (austenite – δ-ferrite) boundaries, dislocations, and similar features [15; 16]. The peak intensity for AM-ASS samples surpasses that of AM-ASS + HT samples, wherein the latter category bears a reduced proportion of the δ-phase. Hence, under analogous saturation conditions, a lesser amount of hydrogen dissolves within AM-ASS + HT samples. This disparity might arise due to the diminished presence of interphase boundaries in the annealed samples, which are capable of adsorbing hydrogen atoms. Given that the diffusion coefficient of hydrogen in δ-ferrite is significantly higher and its solubility lower than in the austenite phase [17; 18], the elevated volume fraction of the δ-phase, along with its morphology characterized by extended continuous lamellae in AM-ASS samples, expedites the profound penetration of hydrogen atoms into the samples during saturation. Put differently, the δ-ferrite branches serve as preferential conduits for the inward transport of hydrogen atoms, contributing to a more effective accumulation of hydrogen within the material (primarily within austenite). This proposition also correlates with the observation of the TDS peak shifting towards higher temperatures for AM-ASS samples in comparison to the peak for AM-ASS + HT samples. This shift could be attributed to a deeper saturation of the samples with hydrogen as the ferrite proportion increases.

Fig. 2, *b* delineates stress-strain diagrams in engineering coordinates for AM-ASS and AM-ASS + HT samples. Mechanical properties ($\sigma_{0.2}$ – yield strength; σ_u – ultimate strength; δ – elongation to fracture; $I_H = \left(\frac{\delta_0 - \delta_H}{\delta_0}\right) \cdot 100$ %; δ_0 and δ_H – elongation to fracture of unhydrogenated and hydrogenated samples) are summarized in Table.

Examination of the provided experimental data demonstrates that post-production heat treatment yields an increase in elongation to failure and a decrease in yield strength for the examined steel. This phenomenon can be attributed to a decrease in the volume fraction of δ-ferrite, as δ-ferrite possesses higher strength compared to austenite [19]. Additionally, there is a reduction in the density of interphase boundaries (austenite – δ-ferrite), which function as barriers to the movement of dislocations during deformation [6].

The process of hydrogen charging induces alterations in the mechanical properties of EBAM steel (outlined in Table). Irrespective of the ferrite content, the yield strength ($\sigma_{0.2}$) of hydrogen-charged samples surpasses that of the original samples (deformed without hydrogen charging). This experimental observation signifies solid-solution hardening of the auste-

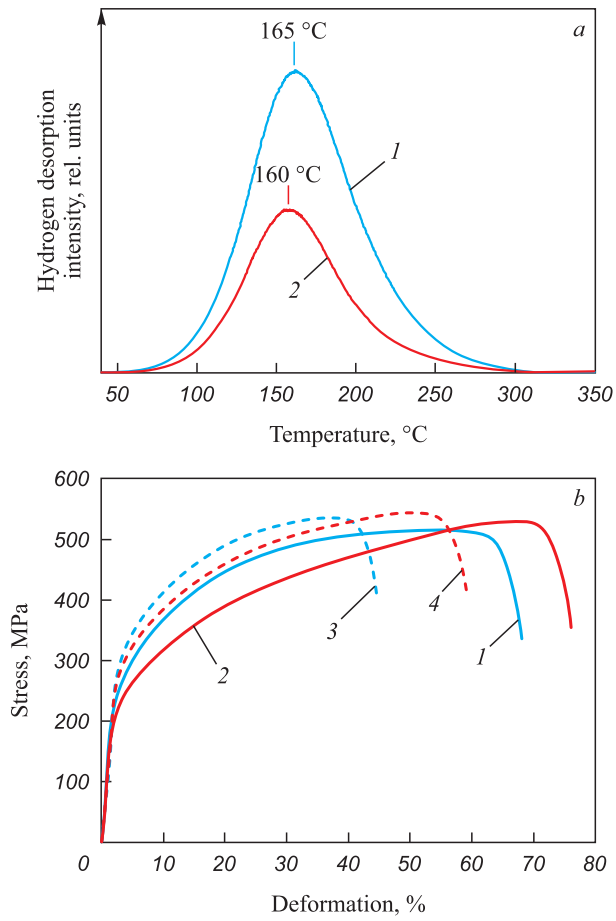

Fig. 2. Thermodesorbtion spectra (*a*) and stress–strain diagrams in engineering coordinates (*b*) (H – hydrogen-charging):
1 and *3* –AM-ASS before and after hydrogen-charging;
2 and *4* – AM-ASS + HT before and after hydrogen-charging

Рис. 2. ТДС-спектры (*a*), а также диаграммы напряжение – деформация в инженерных координатах (*b*) (Н – наводороживание):
1 и *3* – АП-АНС до и после насыщения водородом;
2 и *4* – АП-АНС + ТО до и после насыщения водородом

nitic phase due to the presence of hydrogen atoms [20]. Notably, it's noteworthy that in AM-ASS + HT samples, the hydrogen-induced enhancement in yield strength ($\Delta\sigma^{H}_{0.2}$ = 73 MPa) exceeds that in AM-ASS samples ($\Delta\sigma^{H}_{0.2}$ = 55 MPa), even though, as per the results of TDS analysis, the hydrogen concentration in the latter is higher (Fig. 2, *a*). The presence of a limited volume fraction of ferrite and interfacial boundaries, which function as traps for hydrogen atoms [21], can lead to a heightened accumulation of hydrogen within the austenite grain bodies located near the saturable surface of AM-ASS + HT samples. This accumulation contributes to their solid solution hardening. On the contrary, hydrogen transport is more restricted in AM-ASS + HT samples due to the altered morphology and reduced volume fraction of ferrite, which leads to the suppression of hydrogen transport over long distances along ferrite dendrites and a decrease in the prevalence of interfacial boundaries. Consequently, AM-ASS samples amass a greater total hydrogen concentration. In these samples, the concentration gradient across depth is evidently smaller, subsequently yielding a lower level of solid solution strengthening in the austenite phase compared to AM-ASS + HT samples where hydrogen transport is curtailed. In addition to solid solution hardening, the hydrogen concentration gradient throughout the depth is intrinsically linked to the stress gradient within the tested samples – stemming from their heterogeneous hydrogen charging. This aspect becomes more pronounced in AM-ASS + HT samples where the transfer of hydrogen atoms during charging and subsequent deformation is hindered due to the alterations in morphology and the reduction in the volume fraction of ferrite [22; 23]. Therefore, even with a lower hydrogen adsorption concentration during hydrogen charging, the yield strength of AM-ASS + HT samples, wherein hydrogen transport is limited, displays increased susceptibility to hydrogen charging: the hydrogen-induced rise in yield strength is more significant in AM-ASS + HT samples compared to AM-ASS samples. However, the hydrogen embrittlement factor I_H, which quantifies the reduction in elongation to failure due to hydrogenation, is greater for AM-ASS samples (Table).

Effect of hydrogen-charging on mechanical properties of AM-ASS and AM-ASS +HT samples

Влияние наводороживания на механические свойства образцов АП-АНС и АП-АНС + ТО

Sample	$\sigma_{0.2}$, MPa	σ_u, MPa	δ, %	I_H, %
AM-ASS	220 ± 5	516 ± 7	62 ± 2	32
AM-ASS + H	275 ± 5	537 ± 2	42 ± 2	
AM-ASS + HT	192 ± 4	523 ± 8	73 ± 3	24
AM-ASS + HT + H	265 ± 3	544 ± 3	55 ± 2	

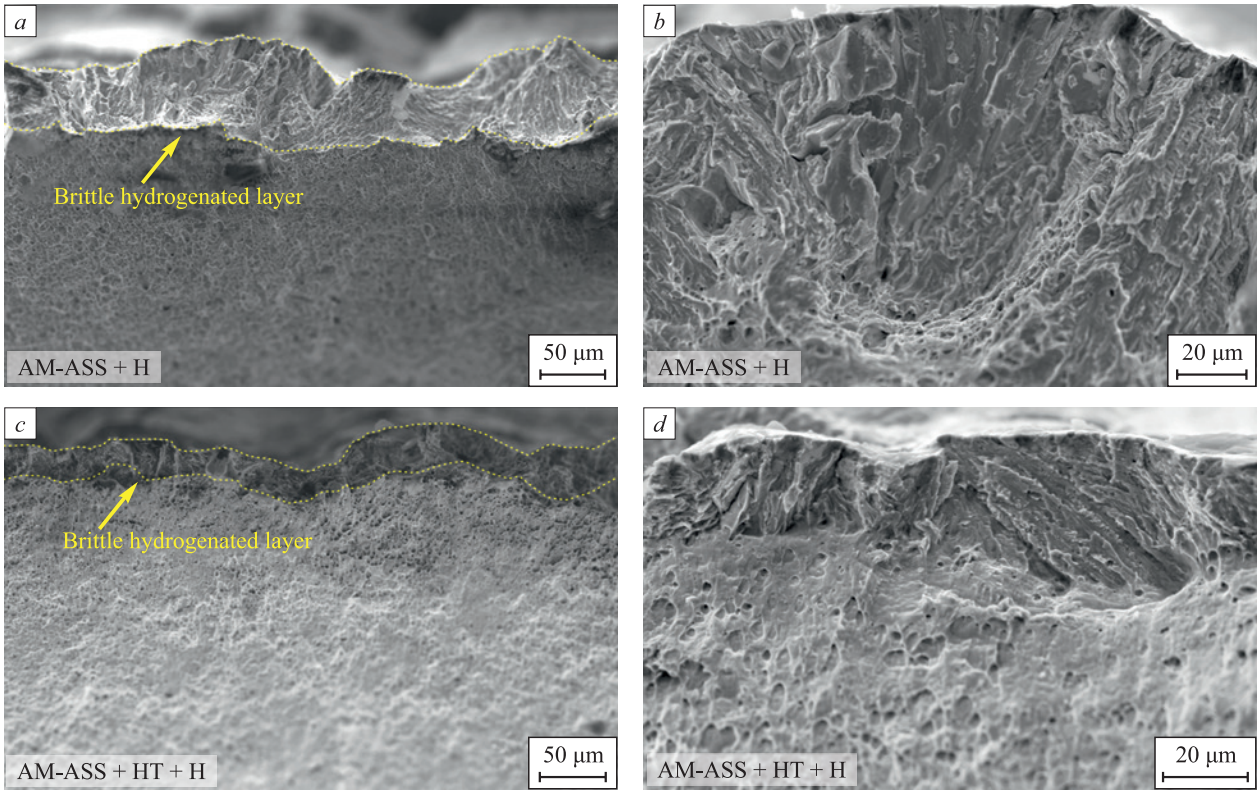

Fig. 3. SEM images of fracture surfaces of hydrogen-charged (H) AM-ASS (*a*, *b*) and AM-ASS + HT (*c*, *d*) samples

Рис. 3. СЭМ-изображения поверхностей разрушения наводороженных (Н) АП-АНС (*a*, *b*) и АП-АНС + ТО (*c*, *d*) образцов

Fig. 3 portrays SEM images of fractured surfaces from both hydrogen-charged AM-ASS and AM-ASS + HT samples. Across all samples, hydrogen charging results in the formation of a brittle surface layer, while the remaining portions of the samples exhibit a ductile transcrystalline fracture mode, comparable to uncharged samples [14].

The fracture surfaces of the brittle hydrogenated layer exhibit features characteristic of both transcrystalline and intercrystalline fracture, including ridges and flat facets. The presence of intercrystalline cleavages aligns with the aforementioned mechanisms of hydrogen adsorption, specifically pointing towards the accumulation of hydrogen atoms at interphase boundaries. The transcrystalline nature of the fracture signifies the brittle fracture of hydrogen-saturated austenite grains, along with the formation of deformation-induced martensite within them, as documented in [2; 14; 23; 24].

The thickness of the brittle hydrogenated layer is notably greater for AM-ASS samples ($D_H = 55 \pm 12$ μm) characterized by a higher initial proportion of ferrite – than for AM-ASS + HT samples ($D_H = 29 \pm 7$ μm). This experimental observation corroborates the findings from TDS studies, mechanical tests, and the preceding discussions.

Conclusions

The investigation delved into the hydrogen embrittlement characteristics of austenitic chromium-nickel steel samples produced via electron beam additive manufacturing in two distinct states: immediately following additive growth and subsequent post-production heat treatment. Annealing the additively manufactured samples at 1100 °C for 1 h yielded a notable reduction in the volume fraction of δ-ferrite – from 20 % to 5 % – accompanied by an alteration in its morphology. Specifically, the state after EBAM exhibited thin extended lamellae of dendrites, while the heat-treated samples showcased isolated inclusions (particles) of ferrite. This transformation in phase composition and microstructure exerted an impact on the steel's susceptibility to hydrogen embrittlement, the solubility and distribution of hydrogen during the process of electrolytic saturation, and the dimensions of the brittle hydrogenated layer within the samples.

Even though the annealed samples with a lower proportion of ferrite contained a lower overall concentration of dissolved hydrogen, their hydrogen-induced increase in yield strength ($\Delta\sigma_{0.2}^{H} = 73$ MPa), exceeded that of samples following EBAM, characterized by a higher proportion of dendritic ferrite ($\Delta\sigma_{0.2}^{H} = 55$ MPa). This discrepancy can be attributed to the impedance of hydrogen transport deep into the samples along δ-ferrite dendrites due to modifications in their morphology and the reduction of interphase boundaries. These boundaries function as traps for hydrogen atoms within both the austenite crystal lattice and intergranular regions. Consequently, post heat treatment, hydrogen transport deep into the samples is curtailed, leading to its accumulation in the surface layers. This accumulation contributes to robust solid-solution hardening of the austenitic phase, thereby engendering a pronounced stress gradient due to the hydrogen concentration gradient in these samples.

The thickness of the brittle hydrogenated surface layer and the hydrogen embrittlement factor were found to be more significant for the initial additively manufactured steel samples ($D_H = 55 \pm 12$ μm, $I_H = 32$ % for AM-ASS and $D_H = 29 \pm 7$ μm, $I_H = 24$ % for AM-ASS + HT samples). The reduction in the volume fraction and the alteration in the morphology of δ-ferrite, brought about by post-production heat treatment, enhance the resistance of EBAM stainless steel to hydrogen embrittlement.

References / Список литературы

1. Michler T., Naumann J. Hydrogen embrittlement of Cr–Mn–N-austenitic stainless steels. *International Journal of Hydrogen Energy*. 2010;35(3):1485–1492. https://doi.org/10.1016/j.ijhydene.2009.10.050
2. Xu X., An J., Wen C., Niu J. Study on the hydrogen embrittlement susceptibility of AISI 321 stainless steel. *Engineering Failure Analysis*. 2021;122:105212. https://doi.org/10.1016/j.engfailanal.2020.105212
3. Bajaj P., Hariharan A., Kini A., Kurnsteiner P., Raabe D., Jagle E.A. Steels in additive manufacturing: A review of their microstructure and properties. *Materials Science and Engineering: A*. 2020;772:138633. https://doi.org/10.1016/j.msea.2019.138633
4. Li N., Huang S., Zhang G., Qin R.Y., Liu W., Xiong H., Shi G., Blackburn J. Progress in additive manufacturing on new materials: A review. *Journal of Materials Science & Technology*. 2019;35(2):242–269. https://doi.org/10.1016/j.jmst.2018.09.002
5. Tarasov S.Yu., Filippov A.V., Shamarin N.N., Fortuna S.V., Maier G.G., Kolubaev E.A. Microstructural evolution and chemical corrosion of electron beam wire-feed additively manufactured AISI 304 stainless steel. *Journal of Alloys and Compounds*. 2019;803:364–370. https://doi.org/10.1016/j.jallcom.2019.06.246
6. Astafurova E.G., Panchenko M.Yu., Moskvina V.A., Maier G.G., Astafurov S.V., Melnikov E.V., Fortuna A.S., Reunova K.A., Rubtsov V.E., Kolubaev E.A. Microstructure and grain growth inhomogeneity in austenitic steel produced by wire-feed electron beam melting: the effect of post-building solid-solution treatment. *Journal of Materials Science*. 2020;55:9211–9224. https://doi.org/10.1007/s10853-020-04424-w
7. Chen X., Li J., Cheng X., He B., Wang H., Huang Zh. Microstructure and mechanical properties of the austenitic stainless steel 316L fabricated by gas metal arc additive manufacturing. *Materials Science and Engineering: A*. 2017;703:567–677. https://doi.org/10.1016/j.msea.2017.05.024

8. Kolubaev E.A., Rubtsov V.E., Chumaevskii A.V., Astafurova E.G. Scientific approaches to micro-, meso- and macrostructural design of bulk metallic and polymetallic materials by wire-feed electron-beam additive manufacturing. *Fizicheskaya mezomekhanika*. 2022;25(4):5–18. (In Russ.). https://doi.org/10.55652/1683-805X_2022_25_4_5

Колубаев Е.А., Рубцов В.Е., Чумаевский А.В., Астафурова Е.Г. Научные подходы к микро-, мезо- и макроструктурному дизайну объемных металлических и полиметаллических материалов с использованием метода электронно-лучевого аддитивного производства. *Физическая мезомеханика*. 2022;25(4):5–18. https://doi.org/10.55652/1683-805X_2022_25_4_5

9. Astafurov S., Astafurova E. Phase composition of austenitic stainless steels in additive manufacturing: A review. *Metals*. 2021;11(7):1052. https://doi.org/10.3390/met11071052

10. Baek S.W., Song E.J., Kim J.H., Jung M., Baek U.B., Nahm S.H. Hydrogen embrittlement of 3-D printing manufactured austenitic stainless steel part for hydrogen service. *Scripta Materialia*. 2017;130:87–90. https://doi.org/10.1016/j.scriptamat.2016.11.020

11. Li S., Liu M., Ren Y., Wang Y. Hydrogen embrittlement behaviors of additive manufactured maraging steel investigated by in situ high-energy X-ray diffraction. *Materials Science and Engineering: A*. 2019;766:138341. https://doi.org/10.1016/j.msea.2019.138341

12. Alnajjar M., Christien F., Bosch C., Wolski K. A comparative study of microstructure and hydrogen embrittlement of selective laser melted and wrought 17–4PH stainless steel. *Materials Science & Engineering: A*. 2020;785:139363. https://doi.org/10.1016/j.msea.2020.139363

13. Panchenko M.Yu., Mel'nikov E.V., Astafurov S.V., Reunova K.A., Kolubaev E.A., Astafurova E.G. Features of hydrogen embrittlement of low-carbon steel obtained by electron beam additive manufacturing. *Izvestiya vuzov. Fizika*. 2022;65(6):53–60. (In Russ.). https://doi.org/10.17223/00213411/65/6/53

Панченко М.Ю., Мельников Е.В., Астафуров С.В., Реунова К.А., Колубаев Е.А., Астафурова Е.Г. Особенности водородного охрупчивания низкоуглеродистой стали, полученной методом электронно-лучевого аддитивного производства. *Известия вузов. Физика*. 2022;65(6):53–60. https://doi.org/10.17223/00213411/65/6/53

14. Yin Q., Chen G., Cao H., Zhang G., Zhang B., Wei S. Transformation law of microstructure evolution and mechanical properties of electron beam freeform fabricated 321 austenitic stainless steel. *Vacuum*. 2021;194:110594. https://doi.org/10.1016/j.vacuum.2021.110594

15. Depover T., Verbeken K. The effect of TiC on the hydrogen induced ductility loss and trapping behavior of Fe–C–Ti alloys. *Corrosion Science*. 2016;112:308–326. https://doi.org/10.1016/j.corsci.2016.07.013

16. Escobar P.D., Depover T., Duprez L., Verbeken K., Verhaege M. Combined thermal desorption spectroscopy, differential scanning calorimetry, scanning electron microscopy and X-ray diffraction study of hydrogen trapping in cold deformed TRIP steel. *Acta Materialia*. 2012;60(6-7):2593–2605. https://doi.org/10.1016/j.actamat.2012.01.026

17. Claeys L., Depover T., De Graeve I., Verbeken K. Electrochemical hydrogen charging of duplex stainless steel. *Corrosion*. 2019;75(8):880–887. https://doi.org/10.5006/2959

18. Owczarek E., Zakroczymski T. Hydrogen transport in a duplex stainless steel. *Acta Materialia*. 2000;48(12):3059–3070. https://doi.org/10.1016/S1359-6454(00)00122-1

19. Abraham D.P., Altstetter C.J. The effect of hydrogen on the yield and flow stress of an austenitic stainless steel. *Metallurgical and Materials Transactions A*. 1995;26:2849–2858. https://doi.org/10.1007/BF02669643

20. Alvarez-Armas I., Degallaix-Moreuil S. *Duplex Stainless Steels*. Wiley-ISTE; 2009:464.

21. Panchenko M.Yu., Melnikov E.V., Mikhno A.S., Maier G.G., Astafurov S.V., Moskvina V.A., Reunova K.A., Galchenko N.K., Astafurova E.G. The influence of intergranular and interphase boundaries and δ-ferrite volume fraction on hydrogen embrittlement of high-nitrogen steel. *International Journal of Hydrogen Energy*. 2021;46(59):30510–30522. https://doi.org/10.1016/j.ijhydene.2021.06.183

22. Brass A.M., Chêne J. Hydrogen uptake in 316L stainless steel: Consequences on the tensile properties. *Corrosion Science*. 2006;48(10):3222–3242. https://doi.org/10.1016/j.corsci.2005.11.004

23. Hahnenberger F., Smaga M., Eifler D. Influence of γ–α'-phase transformation in metastable austenitic steels on the mechanical behavior during tensile and fatigue loading at ambient and lower temperatures. *Advanced Engineering Materials*. 2012;14(10):853–858. https://doi.org/10.1002/adem.201100341

24. Koyama M., Tasan C.C., Tsuzaki K. Overview of metastability and compositional complexity effects for hydrogen-resistant iron alloys: Inverse austenite stability effects. *Engineering Fracture Mechanics*. 2019;214:123–133. https://doi.org/10.1016/j.engfracmech.2019.03.049

Information about the Authors / Сведения об авторах

Marina Yu. Panchenko, *Junior Researcher of the Laboratory of Physics of Hierarchical Structures in Metals and Alloys,* Institute of Strength Physics and Materials Science, Siberian Branch of Russian Academy of Sciences
ORCID: 0000-0003-0236-2227
E-mail: Panchenko.marina4@gmail.com

Kseniya A. Reunova, *Postgraduate, Junior Researcher of the Laboratory of Physics of Hierarchical Structures in Metals and Alloys,* Institute of Strength Physics and Materials Science, Siberian Branch of Russian Academy of Sciences
ORCID: 0000-0002-1318-1010
E-mail: reunova.ksenya@mail.ru

Марина Юрьевна Панченко, *младший научный сотрудник лаборатории физики иерархических структур в металлах и сплавах,* Институт физики прочности и материаловедения Сибирского отделения РАН
ORCID: 0000-0003-0236-2227
E-mail: Panchenko.marina4@gmail.com

Ксения Андреевна Реунова, *аспирант, младший научный сотрудник лаборатории физики иерархических структур в металлах и сплавах,* Институт физики прочности и материаловедения Сибирского отделения РАН
ORCID: 0000-0002-1318-1010
E-mail: reunova.ksenya@mail.ru

***Aleksei S. Nifontov*,** *Research Laboratory Assistant of the Laboratory of Physics of Hierarchical Structures in Metals and Alloys,* Institute of Strength Physics and Materials Science, Siberian Branch of Russian Academy of Sciences
ORCID: 0000-0003-2473-8504
E-mail: trymailzero@gmail.com

***Evgenii A. Kolubaev*,** *Dr. Sci. (Eng.), Director,* Institute of Strength Physics and Materials Science, Siberian Branch of the Russian Academy of Sciences
ORCID: 0000-0001-7288-3656
E-mail: eak@ispms.tsc.ru

***Elena G. Astafurova*,** *Dr. Sci. (Phys.-Math.), Assist. Prof., Head of the Laboratory of Physics of Hierarchical Structures in Metals and Alloys,* Institute of Strength Physics and Materials Science, Siberian Branch of Russian Academy of Sciences
ORCID: 0000-0002-1995-4205
E-mail: elena.g.astafurova@ispms.ru

***Алексей Сергеевич Нифонтов*,** *лаборант-исследователь лаборатории физики иерархических структур в металлах и сплавах,* Институт физики прочности и материаловедения Сибирского отделения РАН
ORCID: 0000-0003-2473-8504
E-mail: trymailzero@gmail.com

***Евгений Александрович Колубаев*,** *д.т.н., директор,* Институт физики прочности и материаловедения Сибирского отделения РАН
ORCID: 0000-0001-7288-3656
E-mail: eak@ispms.tsc.ru

***Елена Геннадьевна Астафурова*,** *д.ф.-м.н., доцент, заведующий лабораторией физики иерархических структур в металлах и сплавах,* Институт физики прочности и материаловедения Сибирского отделения РАН
ORCID: 0000-0002-1995-4205
E-mail: elena.g.astafurova@ispms.ru

Contribution of the Authors

M. Yu. Panchenko – literary review, analysis of the research results, writing the text, design of the article.
K. A. Reunova – literary review, conducting microstructural studies, analysis of the research results.
A. S. Nifontov – preparation of the test samples, analysis and graphical presentation of the research results.
E. A. Kolubaev – scientific guidance, reviewing and editing the article final version.
E. G. Astafurova – formation of the basic concept, scientific guidance, revision of the text.

Вклад авторов

М. Ю. Панченко – обзор литературы, анализ результатов, написание текста статьи, оформление статьи.
К. А. Реунова – обзор литературы, микроструктурные исследования и анализ результатов исследований.
А. С. Нифонтов – подготовка образцов для исследований, анализ и графическое представление результатов.
Е. А. Колубаев – научное руководство исследованиями, редактирование финальной версии статьи.
Е. Г. Астафурова – формирование основной концепции, научное руководство исследованиями, доработка текста.

Received 11.11.2022
Revised 25.11.2022
Accepted 20.04.2023

Поступила в редакцию 11.11.2022
После доработки 25.11.2022
Принята к публикации 20.04.2023